IEEE Access
Multidisciplinary | Rapid Review | Open Access Journal

Received 15 February 2024, accepted 20 March 2024, date of publication 28 March 2024, date of current version 3 April 2024.

Digital Object Identifier 10.1109/ACCESS.2024.3382708

RESEARCH ARTICLE

Closed-Form Dyadic Green's Functions for Dipole Excitation of Planar Periodic Structures

SÜLEYMAN ADANIR AND LALE ALATAN, (Member, IEEE)
Department of Electrical and Electronics Engineering, Middle East Technical University, 06800 Ankara, Turkey
Corresponding author: Lale Alatan (lalatan@metu.edu.tr)

ABSTRACT The analysis of a single source in the vicinity of periodic structures is a very challenging task since the aperiodic source forbids a direct application of a periodic analysis method to the problem. Full wave methods addressing these problems involve infinite summations and double integrations which make the analysis cumbersome. Homogenization based methods reduce this complexity but at the expense of a loss of accuracy and flexibility in handling different kinds of structures. Moreover, the resulting Green's functions still need integrations as opposed to being in closed-form. In this paper, a novel approach is proposed to obtain closed-form expressions for the Green's functions of single sources over periodic structures which makes the analysis of these problems efficient while offering more accuracy and flexibility compared to existing homogenization methods in the literature. To compute the fields scattered by the periodic structure, the reflection coefficients are numerically computed for TE and TM polarized incident plane waves with different angles of incidence and they are approximated by complex exponentials. Approximated reflection coefficients are used in conjunction with the plane wave expansion of the fields radiated by the dipole so that the scattered fields can be expressed in closed-form by utilizing Bessel integral identities.

INDEX TERMS Closed-form dyadic Green's functions, planar periodic structures, multilayered media, electric dipole excitation, method of moments.

I. INTRODUCTION

Aperiodic sources placed over periodic structures have attracted great interest from researchers of electromagnetics area. High-impedance surfaces (HIS), which are also referred to as reactive impedance surfaces (RIS) or artificial magnetic conductors (AMC), are special types of metasurfaces originally proposed in [1]. It is generally utilized in antenna applications to improve its radiation characteristics, such as reduced size [2], [3], increased side-lobe suppression [4], enhanced bandwidth [5], reduced mutual coupling [6] and wider scanning angles [7]. They have also found use in design of endfire antennas [8], [9], low profile multi-beam omnidirectional antennas [10] and null-steering antennas with deep nulls in wide bandwidths [11]. All these important applications utilize HIS in the vicinity of the antenna which provides the motivation behind the interest of researchers in analyzing electric dipole sources over planar periodic structures printed on multilayered media.

Plane-wave expansion method (PWM), a good summary of which can be found in [12], is a well established technique in electromagnetics literature which can be used to tackle the problem of dipole excitation of periodic structures. It relies on the fact that a spherical wave can be written as an integral summation of plane waves. This integration is actually a 2D inverse Fourier transformation and also known as Weyl Identity [13]. In order to find the scattered electric field due to a unit amplitude incident plane wave, electric field integral equation (EFIE) is utilized. By superposition, the weighted integral of these scattered fields yield the total scattered field due to the dipole source. EFIE formulation involves the periodic Green's function (PGF) of the structure which is expressed as a double infinite spectral summation. Thus, calculation of the scattered field due to the dipole source involves a double infinite integral and a double infinite summation when the plane-wave expansion method is employed.

The associate editor coordinating the review of this manuscript and approving it for publication was Ladislau Matekovits.

Array scanning method (ASM) [14], [15], [16] can be utilized to reduce the limits of the double integration to finite values. This method is based on synthesizing the single dipole source from an infinite phased array of dipole sources with periodicity same as the periodicity of the structure. By converting the single source to an infinite phased array of sources, ASM opens the way of utilizing an efficient periodic moment method to find the scattered fields for infinite array. The response of the single dipole can be obtained by integrating the phased array expression over the Brillouin zone ($\pm\pi$/periodicity). Thus, ASM involves double infinite summation and 2D finite integration for the analysis of a single source placed over a periodic structure.

Array scanning method was applied for the problem of calculating the fields of a line source above a 1-D periodic structure in [17] and for the problem with a line source above a 2-D periodic structure in [18]. The problem with a dipole source over 2-D periodic structure is investigated in [12].

ASM, while being highly accurate and more efficient compared to PWM, is still not a highly efficient technique especially when it comes to analyzing fields for many different source and observation positions. As a way of overcoming this efficiency issue in full-wave approaches, researchers worked on homogenization based methods which rely on the characterization of metasurfaces by generalized sheet transition conditions (GSTCs) [19] which can be expressed in terms of surface susceptibilities [20], [21], [22], [23], [24], [25], [26] or surface impedance matrices [27], [28], [29].

Homogenization based approaches were applied for the problem of calculating the fields of a line source above a 1-D periodic structure in [30] and for the problem with a line source above a 2-D periodic structure in [31]. To the best of our knowledge, first study on homogenized Green's functions for the problem with a dipole source over 2-D periodic structure is [32].

In [32], the Green's functions for the fields in both sides of the interface are expressed as double integrations in the spectral domain that contains reflection and transmission coefficients. To find the unknown coefficients, boundary conditions are applied which are actually GSTCs that can be in terms of surface susceptibilities or impedances. After solving the equations for the unknowns, the reflection and transmission coefficients are put in the expressions of Green's functions and 2D integrations in spectral domain are carried out to obtain the field values due to the dipole source.

The authors of [32] presented expressions for reflection and transmission coefficients obtained by surface susceptibility approach and also surface impedance approach. However, this formulation is given for the special case of a homogeneous background and isotropic structures. As for the numerical results, dipole excitation of periodic square PEC patches in free space is studied. Susceptibilities and surface impedances are obtained from analytical closed form expressions in the literature. They compared their results to the results from ASM which is considered to be exact up to the numerical accuracy. It is reported that their results are in agreement with the full-wave ASM results when periodicity is smaller than 0.1λ and distances of the source and observation points to the surface are larger than the periodicity. However, the accuracy of the method can not be clearly evaluated since, instead of the scattered field values, the total field values which are heavily dominated by the incident field for the given parameters of the studied problem are presented.

The approach in [32] is extended for metafilms at the interface of two half spaces in [33] and for metasurfaces placed on a dielectric slab in [34]. Since the numerical results are reported for total fields, a significant difference between the results for two different dielectric constants (5 and 16), [33], and for two slabs of same permittivity but with different heights (2 mm and 10 mm), [34], is not observed again due to the dominance of the incident field.

Even though homogenization based approaches offer efficient solutions, the accuracy of the scattered fields due to a dipole source near 2-D periodic structures obtained by homogenized Green's function approach is not explicitly verified in literature as explained in the previous paragraphs. Moreover in [21], in which the reflection and transmission properties of a metasurface homogenized by surface susceptibilities are studied, the authors state that the fields appearing in the GSTCs are ''macroscopic'' fields which mean that they do not exhibit variations on a length scale comparable to scatterer dimensions or spacing, but only on larger scales such as the wavelength in the surrounding medium. This statement means that the scattered fields obtained by homogenized Green's function approaches based on GSTCs will fail to accurately represent the actual field variations, which limits its usage to the applications where approximate field values on the scales of a wavelength are sufficient. On the other end, the fields obtained by using full wave approaches such as PWM or ASM will be highly accurate but at the expense of exhaustive computation power and time. Note that, neither full wave nor the homogenization based approaches yield closed form solutions which means it is necessary to carry out integrations and summations for each different pair of source and observation point.

In this paper, a novel approach is proposed that provides closed form expressions to calculate the scattered fields due to the electric dipole source placed close to planar periodic structures in a more efficient way than the available full wave methods in the literature while keeping the accuracy at high levels even for the field variations within the fraction of a wavelength as opposed to the currently available homogenization based approaches. The proposed approach is applicable to problems whose parameters satisfy the same conditions in which homogenization methods are valid: i) the periodicity is sufficiently small compared to wavelength ($< 0.1\lambda$), so that the higher-order Floquet modes

are negligible, ii) the observation point is not too close (distance smaller than periodicity) to the periodic structure.

The formulation of the proposed approach will be introduced in Section II, followed by the numerical examples presented in Section III. Section IV will include the concluding remarks.

II. FORMULATION

Calculation of reflected fields from the periodic structure when excited by plane wave is a crucial step in the approach proposed in this paper. Therefore, this analysis is shortly introduced in II-A and the formulation for the main problem is detailed in II-B.

A. REFLECTION COEFFICIENT ANALYSIS

Electric fields scattered by infinite periodic structures, lying on a plane transverse to z and excited by a plane wave incident in (θ_i, ϕ_i), can be expressed in the form of an infinite spectral summation as [35] and [36]:

$$\vec{E}^s(\vec{r}, \vec{r'}) = \sum_{p=-\infty}^{+\infty} \sum_{q=-\infty}^{+\infty} \vec{E}_{pq}(k_{xp}, k_{yq}, \vec{r'}) e^{-j(k_{xp}x + k_{yq}y + k_{zpq}z)} \tag{1}$$

where transverse and longitudinal wavenumbers are defined below as:

$$k_{xp} = k_x + \frac{2\pi p}{D_x} \quad , \quad k_{yq} = k_y + \frac{2\pi q}{D_y} \tag{2}$$

$$k_{zpq} = \begin{cases} \sqrt{k_s^2 - (k_{xp}^2 + k_{yq}^2)} & k_s^2 \geq k_{xp}^2 + k_{yq}^2 \\ -j\sqrt{(k_{xp}^2 + k_{yq}^2) - k_s^2} & k_s^2 \leq k_{xp}^2 + k_{yq}^2 \end{cases} \tag{3}$$

k_s is the wavenumber in the medium whereas k_x $(= k_s \sin\theta_i \cos\phi_i)$ and k_y $(= k_s \sin\theta_i \sin\phi_i)$ are the transverse wavenumbers of the incident wave. D_x and D_y are the periodicities (spacing between elements) in x and y directions, respectively.

The exponential term inside the summation in (1) is known as a Floquet mode or a Floquet modal function [35]. Electromagnetic fields can be decomposed into Transverse Electric (TE) and Transverse Magnetic (TM) parts with respect to the plane of incidence based on a definition of unit electric field vectors for these two orthogonal modes. TE and TM reflection coefficients of the periodic structures are calculated by exciting the structure with a unit amplitude TE or TM plane wave. This analysis is generally performed by using the concept of S-parameters with S_{ij} convention where i refers to the index of the reflected wave while j refers to the incident wave. Indices 1 and 2 refer to the TE and TM polarized fundamental $(p = 0, q = 0)$ Floquet mode, respectively. Indices greater than 2 refer to TE or TM polarized components of higher order Floquet modes which are sorted according to their complex wavenumber in z direction.

Calculation of the reflected TE and TM fields is carried out by applying Method of Moment (MoM) technique to solve Mixed Potential Integral Equation (MPIE). RWG basis function introduced in [37] is preferred in this work for its flexibility in handling arbitrary geometries while Galerkin method is utilized where the testing function is the same as the basis function.

MoM analysis requires the Green's function of the structure which is a slowly convergent series for periodic multilayered structures. This challenge is circumvented by combining 3-level Discrete Complex Image Method (DCIM) [38] and Ewald [39] techniques, a combination which has a proven accuracy and efficiency as demonstrated in our previous work [40].

B. DIPOLE EXCITATION OF PERIODIC STRUCTURES

A simple illustration of the problem is given in Fig. 1. The point of observation is shown as $\vec{r}_o$ and the location of the electric dipole source is $\vec{r}_d$. The electric dipole current source oriented along the direction $\hat{a}_j$ can be expressed as follows:

$$\vec{J}_d(\vec{r'}) = \hat{a}_j \delta(\vec{r'} - \vec{r}_d) \tag{4}$$

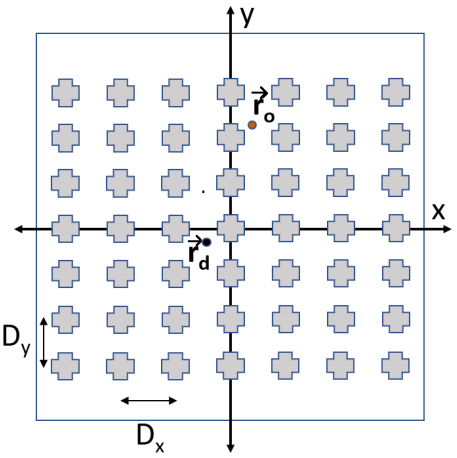

FIGURE 1. Periodic structure with a rectangular lattice of PEC scatterers with spacings D_x and D_y, excited by a dipole source at point $\vec{r}_d$.

The electric fields associated with this source provide Green's functions of the structure since it is a point dipole source with unit amplitude. This Green's function is not a scalar but rather a dyadic entity since such a source in a given direction creates fields in all three directions. The following formulation is for deriving the components of this dyadic Green's function due to horizontal dipole sources.

As described in the previous section, the response (reflection coefficients) of the planar periodic structure can be obtained for plane wave incidence. Thus, the formulation starts with expressing the spherical field radiated by the dipole in terms of its plane wave spectrum as in (5) [12].

$$\vec{E}_{inc}(\vec{r}, \vec{r}_d) = \frac{-j}{8\pi^2} \int\int_{-\infty}^{+\infty} dk_x dk_y \frac{1}{k_z} \bar{\bar{G}}(\vec{k}_\rho) \cdot \hat{a}_j \times e^{-j[k_x(x-x_d) + k_y(y-y_d) + k_z|z-z_d|]} \tag{5}$$

$\bar{\bar{G}}(\vec{k_\rho})$ is a dyad defined in (6) and the wavenumber expressions are given in (7).

$$\bar{\bar{G}}(\vec{k_\rho}) = [-j\omega\mu\bar{\bar{I}} - \frac{1}{j\omega\epsilon}\vec{k}\vec{k}] \tag{6}$$

$$\vec{k} = \hat{a}_x k_x + \hat{a}_y k_y \mp \hat{a}_z k_z \quad ; \quad \vec{k_\rho} = \hat{a}_x k_x + \hat{a}_y k_y \tag{7}$$

The "minus (plus)" sign is used when the observation point is below (above) the source point. For the problem we focus on, the aperiodic source is above the periodic structure and we are interested in the plane waves incident on the periodic structure. Thus, for the incident plane waves, observation point is below the source point and hence the "minus" sign is used in the wavenumber definition. When dealing with the reflected plane waves from the periodic structure, the observation point is above the source (surface currents on the periodic scatterers) point and thus a "plus" sign is used in the wavenumber definition.

Incident electric field is a continuum of plane waves of the form given by equations (8) to (10).

$$\vec{E}^{PW}_{inc}(\vec{r}, \vec{r_d}, \vec{k_\rho}) = \vec{E}_{pwi}(\vec{r}, \vec{r_d}, \vec{k_\rho}) e^{-j[k_x x + k_y y - k_z z]} \tag{8}$$

$$\vec{E}_{pwi}(\vec{k_\rho}, \vec{r_d}) = \bar{\bar{G}}(\vec{k_\rho}) \cdot \hat{a}_j W_{inc}(\vec{k_\rho}, \vec{r_d}) \tag{9}$$

$$W_{inc}(\vec{k_\rho}, \vec{r_d}) = \frac{-j}{8\pi^2}\frac{1}{k_z} e^{j[k_x x_d + k_y y_d - k_z z_d]} \tag{10}$$

The incident field for each plane wave can be written as the sum of its TE and TM components in terms of the unit electric field vectors for TE ($\hat{e}_{te}$) and TM ($\hat{e}_{tmi}$ for incident, $\hat{e}_{tmr}$ for reflected) polarizations as:

$$\vec{E}_{pwi}(\vec{k_\rho}, \vec{r_d}) = E_{te}(\vec{k_\rho}, \vec{r_d})\hat{e}_{te}(\vec{k_\rho}) + E_{tmi}(\vec{k_\rho}, \vec{r_d})\hat{e}_{tmi}(\vec{k_\rho}) \tag{11}$$

$$\hat{e}_{te}(\vec{k_\rho}) = \hat{a}_x \frac{k_y}{k_\rho} + \hat{a}_y \frac{-k_x}{k_\rho} \tag{12}$$

$$\hat{e}_{tmi}(\vec{k_\rho}) = \hat{a}_x \frac{-k_x k_z}{k_\rho k_s} + \hat{a}_y \frac{-k_y k_z}{k_\rho k_s} + \hat{a}_z \frac{-k_\rho}{k_s} \tag{13}$$

$$\hat{e}_{tmr}(\vec{k_\rho}) = \hat{a}_x \frac{-k_x k_z}{k_\rho k_s} + \hat{a}_y \frac{-k_y k_z}{k_\rho k_s} + \hat{a}_z \frac{k_\rho}{k_s} \tag{14}$$

E_{te} and E_{tmi} can be obtained simply by scalar multiplication of $\vec{E}_{pwi}$ with $\hat{e}_{te}$ and $\hat{e}_{tmi}$, respectively, following the fact that $\hat{e}_{te} \cdot \hat{e}_{te} = \hat{e}_{tmi} \cdot \hat{e}_{tmi} = 1$ and $\hat{e}_{te} \cdot \hat{e}_{tmi} = 0$.

$$E_{te,tmi}(\vec{k_\rho}, \vec{r_d}) = \hat{e}_{te,tmi}(\vec{k_\rho}) \cdot [-j\omega\mu\bar{\bar{I}} - \frac{1}{j\omega\epsilon}\vec{k}\vec{k}] \cdot \hat{a}_j W_{inc}(\vec{k_\rho}, \vec{r_d}) \tag{15}$$

Since field vectors are orthogonal to propagation direction, $\hat{e}_{te,tmi} \cdot \vec{k} = 0$ which yields:

$$E_{te,tmi}(\vec{k_\rho}, \vec{r_d}) = -j\omega\mu\hat{e}_{te,tmi}(\vec{k_\rho}) \cdot \hat{a}_j W_{inc}(\vec{k_\rho}, \vec{r_d}) \tag{16}$$

The formulation will be detailed for the y oriented dipole source ($\hat{a}_j = \hat{a}_y$) only, since the derivation for other orientations is straightforward by applying the same procedure. The magnitudes of TE and TM components can be written as:

$$E_{te}(\vec{k_\rho}, \vec{r_d}) = \frac{\omega\mu}{8\pi^2}\frac{k_x}{k_z k_\rho} e^{j[k_x x_d + k_y y_d - k_z z_d]} \tag{17}$$

$$E_{tmi}(\vec{k_\rho}, \vec{r_d}) = E_{tmr}(\vec{k_\rho}, \vec{r_d}) = \frac{\omega\mu}{8\pi^2}\frac{k_y}{k_\rho k_s} e^{j[k_x x_d + k_y y_d - k_z z_d]} \tag{18}$$

By using the unit TE and TM vectors as incident plane waves, S-parameters of the periodic structure (for the fundamental Floquet harmonic) are calculated numerically through the use of MoM as described in Section II-A. E_{te}, E_{tmi} and E_{tmr} values in (17) and (18) and unit vector definitions in (12) - (14) are utilized together with the calculated S parameters of the periodic structure to compute TE and TM polarized reflected waves. Finally, x component of the total scattered electric field due to a y directed electric dipole above the periodic surface can be found as:

$$\begin{aligned} E_{xy}(\vec{r_o}, \vec{r_d}) = \int_{-\infty}^{+\infty}\int \Big\{ & dk_x dk_y e^{-jk_x x_o} e^{-jk_y y_o} e^{-jk_z z_o} \\ & \times \Big[E_{te}(\vec{k_\rho}, \vec{r_d}) S_{11}(\vec{k_\rho}) \frac{k_y}{k_\rho} \\ & + E_{te}(\vec{k_\rho}, \vec{r_d}) S_{21}(\vec{k_\rho}) \frac{-k_x k_z}{k_\rho k_s} \\ & + E_{tmi}(\vec{k_\rho}, \vec{r_d}) S_{12}(\vec{k_\rho}) \frac{k_y}{k_\rho} \\ & + E_{tmi}(\vec{k_\rho}, \vec{r_d}) S_{22}(\vec{k_\rho}) \frac{-k_x k_z}{k_\rho k_s} \Big] \Big\} \end{aligned} \tag{19}$$

$$\begin{aligned} E_{xy}(\vec{r_o}, \vec{r_d}) = \frac{\omega\mu}{8\pi^2} \int_{-\infty}^{+\infty}\int \Big\{ & dk_x dk_y e^{-jk_x(x_o - x_d)} e^{-jk_y(y_o - y_d)} \\ & \times \frac{e^{-jk_z(z_o + z_d)}}{k_z} \Big[\frac{k_x k_y}{k_\rho^2} S_{11}(\vec{k_\rho}) - \frac{k_x^2 k_z}{k_s k_\rho^2} S_{21}(\vec{k_\rho}) \\ & + \frac{k_y^2 k_z}{k_s k_\rho^2} S_{12}(\vec{k_\rho}) - \frac{k_x k_y k_z^2}{k_s^2 k_\rho^2} S_{22}(\vec{k_\rho}) \Big] \Big\} \end{aligned} \tag{20}$$

Similarly, following expressions for y and z components of the total scattered field are obtained.

$$\begin{aligned} E_{yy}(\vec{r_o}, \vec{r_d}) = \frac{\omega\mu}{8\pi^2} \int_{-\infty}^{+\infty}\int \Big\{ & dk_x dk_y e^{-jk_x(x_o - x_d)} e^{-jk_y(y_o - y_d)} \\ & \times \frac{e^{-jk_z(z_o + z_d)}}{k_z} \Big[-\frac{k_x^2}{k_\rho^2} S_{11}(\vec{k_\rho}) - \frac{k_x k_y k_z}{k_s k_\rho^2} S_{21}(\vec{k_\rho}) \\ & - \frac{k_x k_y k_z}{k_s k_\rho^2} S_{12}(\vec{k_\rho}) - \frac{k_y^2 k_z^2}{k_s^2 k_\rho^2} S_{22}(\vec{k_\rho}) \Big] \Big\} \end{aligned} \tag{21}$$

$$\begin{aligned} E_{zy}(\vec{r_o}, \vec{r_d}) = \frac{\omega\mu}{8\pi^2} \int_{-\infty}^{+\infty}\int \Big\{ & dk_x dk_y e^{-jk_x(x_o - x_d)} e^{-jk_y(y_o - y_d)} \\ & \times \frac{e^{-jk_z(z_o + z_d)}}{k_z} \Big[\frac{k_x}{k_s} S_{21}(\vec{k_\rho}) + \frac{k_y k_z}{k_s^2} S_{22}(\vec{k_\rho}) \Big] \Big\} \end{aligned} \tag{22}$$

In order to be able to obtain closed-form expressions, we need to evaluate these 2-D inverse Fourier transform integrals, given in (20)-(22), analytically. Using identities

like Weyl or Sommerfeld helps to achieve this goal. There are branch point singularities in the integration domain at $k_z = 0$ or $k_\rho = k_s$. Since these points form a circle in the Cartesian $k_x - k_y$ plane, they pose a bigger challenge in this domain compared to the cylindrical coordinates. Thus, by using the following change of variables, the integrals are transformed into polar coordinates.

$$\begin{aligned} k_x &= k_\rho \cos(\phi) \quad ; \quad k_y = k_\rho \sin(\phi) \\ x_o - x_d &= \rho \cos(\Psi) \quad ; \quad y_o - y_d = \rho \sin(\Psi) \\ dk_x dk_y &= k_\rho dk_\rho d\phi \end{aligned} \tag{23}$$

When the periodic structure has a symmetry such that the variation of reflection coefficient is negligible for different incident angles in ϕ direction, the reflection coefficient can be assumed to be independent of ϕ. At this point, we limit our attention to such structures whose S-parameters depend only on k_ρ and are independent of ϕ so that the integration with respect to ϕ can be found analytically by using Bessel integral identities given in Appendix A. Starting with the y component of the scattered electric field due to a y oriented dipole, the contribution to $E_{yy}(\vec{r}_o, \vec{r}_d)$ from $S_{11}(k_\rho)$ can be written in cylindrical coordinates as:

$$\begin{aligned} E_{yy}^{S_{11}}(\vec{r}_o, \vec{r}_d) = -\frac{j\omega\mu}{8\pi} \int_0^{+\infty} k_\rho dk_\rho \frac{e^{-jk_z(z_o+z_d)}}{jk_z} S_{11}(k_\rho) \\ \times \frac{1}{\pi} \int_0^{2\pi} d\phi \cos^2(\phi) e^{-jk_\rho \rho \cos(\phi-\Psi)} \end{aligned} \tag{24}$$

The integral with respect to ϕ can be divided into two parts ($I = I_1 + I_2$) as:

$$I_1 = \frac{1}{2\pi} \int_0^{2\pi} d\phi e^{-jk_\rho \rho \cos(\phi-\Psi)} = J_0(k_\rho \rho) \tag{25}$$

$$I_2 = \frac{1}{2\pi} \int_0^{2\pi} d\phi \cos(2\phi) e^{-jk_\rho \rho \cos(\phi-\Psi)} \tag{26}$$

I_2 can be obtained in the following form after using the complex exponential expansion of the cosine function and performing a change of variables ($\phi - \Psi = \psi$).

$$I_2 = -\cos(2\Psi) J_2(k_\rho \rho) \tag{27}$$

The recurrence relation of Bessel functions given in Appendix A is utilized to express the second order Bessel function in terms of lower order counterparts as:

$$J_2(k_\rho \rho) = \frac{2}{k_\rho \rho} J_1(k_\rho \rho) - J_0(k_\rho \rho) \tag{28}$$

Finally, I_2 can also be expressed in terms of zeroth order and first order Bessel functions like I_1.

$$\begin{aligned} I_2 &= I_{2a} + I_{2b} \\ I_{2a} &= \cos(2\Psi) J_0(k_\rho \rho) \\ I_{2b} &= -\frac{2\cos(2\Psi)}{\rho} \frac{1}{k_\rho} J_1(k_\rho \rho) \end{aligned} \tag{29}$$

The reason for preferring zeroth order and first order Bessel function representations is to perform the remaining 1-D integral with respect to k_ρ analytically by using Sommerfeld identity or its derivative with respect to ρ (given in Appendix A). The formulation for the contributions from I_1, I_{2a} and I_{2b} (denoted with a superscript) will be presented separately, starting with contribution of I_1 as:

$$\begin{aligned} E_{yy}^{S_{11}:I_1}(\vec{r}_o, \vec{r}_d) = -\frac{j\omega\mu}{8\pi} \int_0^{+\infty} k_\rho dk_\rho \frac{e^{-jk_z(z_o+z_d)}}{jk_z} S_{11}(k_\rho) \\ \times J_0(k_\rho \rho) \end{aligned} \tag{30}$$

In order to make the integrand compatible with the above mentioned identities, $S_{11}(k_\rho)$ is approximated in terms of complex exponentials by utilizing DCIM [41] as:

$$S_{11}(k_\rho) = \sum_{k=1}^{N_1} B_{1k} e^{-jk_z \gamma_{1k}} \tag{31}$$

Applying the Sommerfeld identity gives us the contribution in a finite summation form as:

$$E_{yy}^{S_{11}:I_1}(\vec{r}_o, \vec{r}_d) = -\frac{j\omega\mu}{8\pi} \sum_{k=1}^{N_1} B_{1k} \frac{e^{-jk_s r_{1k}}}{r_{1k}} \tag{32}$$

where r_{1k} is defined as:

$$r_{1k} = \sqrt{(x_o - x_d)^2 + (y_o - y_d)^2 + (z_o + z_d + \gamma_{1k})^2} \tag{33}$$

Since I_{2a} is just the scaled version of I_1 by $\cos(2\Psi)$, the contribution from I_{2a} can be directly written as:

$$E_{yy}^{S_{11}:I_{2a}}(\vec{r}_o, \vec{r}_d) = -\frac{j\omega\mu}{8\pi} \cos(2\Psi) \sum_{k=1}^{N_1} B_{1k} \frac{e^{-jk_s r_{1k}}}{r_{1k}} \tag{34}$$

I_{2b} can be written in the following form by using (23) and (29) to obtain the integral as:

$$\begin{aligned} E_{yy}^{S_{11}:I_{2b}}(\vec{r}_o, \vec{r}_d) = \frac{j\omega\mu}{8\pi} \frac{2\cos(2\Psi)}{\rho} \int_0^{+\infty} \Bigg\{ dk_\rho k_\rho^2 J_1(k_\rho \rho) \\ \times \frac{e^{-jk_z(z_o+z_d)}}{jk_z} \frac{S_{11}(k_\rho)}{k_\rho^2} \Bigg\} \end{aligned} \tag{35}$$

Note that the derivative of Sommerfeld identity can be utilized to evaluate this integral analytically if this time $\frac{S_{11}(k_\rho)}{k_\rho^2}$ is approximated in terms of complex exponentials as:

$$\frac{S_{11}(k_\rho)}{k_\rho^2} = \sum_{k=1}^{N_{a1}} B_{a1k} e^{-jk_z \gamma_{a1k}} \tag{36}$$

By using this approximation and the derivative form of Sommerfeld identity, the contribution from I_{2b} is written in a finite summation form as:

$$\begin{aligned} E_{yy}^{S_{11}:I_{2b}}(\vec{r}_o, \vec{r}_d) = \frac{j\omega\mu}{4\pi} \cos(2\Psi) \sum_{k=1}^{N_{a1}} \Bigg\{ B_{a1k}(1 + jk_s r_{a1k}) \\ \times \frac{e^{-jk_s r_{a1k}}}{r_{a1k}^3} \Bigg\} \end{aligned} \tag{37}$$

where r_{a1k} is defined as:

$$r_{a1k} = \sqrt{(x_o - x_d)^2 + (y_o - y_d)^2 + (z_o + z_d + \gamma_{a1k})^2} \quad (38)$$

Next we will focus on the contribution of $S_{21}(k_\rho)$ to $E_{yy}(\vec{r}_o, \vec{r}_d)$ and highlight the similarity of the procedure needed to apply for obtaining closed-form expressions. Moreover, for this contribution, the S-parameter related variables that need to be approximated via DCIM will be pointed out and the resultant closed-form expressions will be presented. The contribution of $S_{21}(k_\rho)$ can be written in polar coordinates as:

$$E_{yy}^{S_{21}}(\vec{r}_o, \vec{r}_d) = -\frac{j\omega\mu}{8\pi} \int_0^{+\infty} k_\rho dk_\rho \frac{e^{-jk_z(z_o+z_d)}}{jk_z} \frac{S_{21}(k_\rho)k_z}{k_s} \times \frac{1}{\pi} \int_0^{2\pi} d\phi \cos(\phi)\sin(\phi) e^{-jk_\rho \rho \cos(\phi - \Psi)} \quad (39)$$

By applying a similar procedure as presented above and by using the same change of variables ($\phi - \Psi = \psi$), the integral with respect to ϕ can be obtained as:

$$I = -\sin(2\Psi) J_2(k_\rho \rho) = I_a + I_b$$
$$I_a = \sin(2\Psi) J_0(k_\rho \rho) \quad ; \quad I_b = -\frac{2\sin(2\Psi)}{\rho} \frac{1}{k_\rho} J_1(k_\rho \rho) \quad (40)$$

Due to the similarity of I_a to I_{2a} and I_b to I_{2b} in (29), it is obvious that the remaining 1-D integrals over k_ρ can be obtained in closed form by utilizing Sommerfeld identity and its derivative for I_a and I_b related terms, respectively. In order to utilize these identities the following DCIM approximations are required.

$$\frac{S_{21}(k_\rho)k_z}{k_s} = \sum_{k=1}^{N_2} B_{2k} e^{-jk_z\gamma_{2k}} \quad (41)$$

$$\frac{S_{21}(k_\rho)k_z}{k_s k_\rho^2} = \sum_{k=1}^{N_{a2}} B_{a2k} e^{-jk_z\gamma_{a2k}} \quad (42)$$

The final form of the contribution of $S_{21}(k_\rho)$ can be written as a sum of two finite summations, one for I_a and one for I_b, as:

$$E_{yy}^{S_{21}:I_a}(\vec{r}_o, \vec{r}_d) = -\frac{j\omega\mu}{8\pi} \sin(2\Psi) \sum_{k=1}^{N_2} B_{2k} \frac{e^{-jk_s r_{2k}}}{r_{2k}} \quad (43)$$

$$r_{2k} = \sqrt{(x_o - x_d)^2 + (y_o - y_d)^2 + (z_o + z_d + \gamma_{2k})^2} \quad (44)$$

$$E_{yy}^{S_{21}:I_b}(\vec{r}_o, \vec{r}_d) = \frac{j\omega\mu}{4\pi} \sin(2\Psi) \sum_{k=1}^{N_{a2}} B_{a2k}(1 + jk_s r_{a2k}) \times \frac{e^{-jk_s r_{a2k}}}{r_{a2k}^3} \quad (45)$$

$$r_{a2k} = \sqrt{(x_o - x_d)^2 + (y_o - y_d)^2 + (z_o + z_d + \gamma_{a2k})^2} \quad (46)$$

By observing (21) and noting that $S_{21} = S_{12}$ due to reciprocity, the contribution from S_{12} is exactly the same as the one from S_{21}. Thus,

$$E_{yy}^{S_{12}}(\vec{r}_o, \vec{r}_d) = E_{yy}^{S_{21}}(\vec{r}_o, \vec{r}_d) \quad (47)$$

Finally, to express the contribution of $S_{22}(k_\rho)$ to $E_{yy}(\vec{r}_o, \vec{r}_d)$ in closed-form, the following DCIM approximations are needed.

$$\frac{S_{22}(k_\rho)k_z^2}{k_s^2} = \sum_{k=1}^{N_3} B_{3k} e^{-jk_z\gamma_{3k}} \quad (48)$$

$$\frac{S_{22}(k_\rho)k_z^2}{k_s^2 k_\rho^2} = \sum_{k=1}^{N_{a3}} B_{a3k} e^{-jk_z\gamma_{a3k}} \quad (49)$$

Similar to the contribution of $S_{11}(k_\rho)$, this contribution will also have three components, namely I_1, I_{2a}, I_{2b}, after the analytical evaluation of the integral with respect to ϕ. By using Sommerfeld identity and its derivative, in conjunction with the related DCIM approximations, each component of $S_{22}(k_\rho)$ can be written in closed-form as:

$$E_{yy}^{S_{22}:I_1}(\vec{r}_o, \vec{r}_d) = -\frac{j\omega\mu}{8\pi} \sum_{k=1}^{N_3} B_{3k} \frac{e^{-jk_s r_{3k}}}{r_{3k}} \quad (50)$$

$$r_{3k} = \sqrt{(x_o - x_d)^2 + (y_o - y_d)^2 + (z_o + z_d + \gamma_{3k})^2} \quad (51)$$

$$E_{yy}^{S_{22}:I_{2b}}(\vec{r}_o, \vec{r}_d) = -\frac{j\omega\mu}{4\pi} \cos(2\Psi) \sum_{k=1}^{N_{a3}} B_{a3k}(1 + jk_s r_{a3k}) \times \frac{e^{-jk_s r_{a3k}}}{r_{a3k}^3} \quad (52)$$

$$r_{a3k} = \sqrt{(x_o - x_d)^2 + (y_o - y_d)^2 + (z_o + z_d + \gamma_{a3k})^2} \quad (53)$$

Contribution of I_{2a} can be obtained simply by scaling (50) with $-\cos(2\Psi)$.

We have completed the derivation of closed-form expressions for the y component of scattered electric field due to a y oriented electric dipole over the periodic structure. Derivation for the other transverse component (E_{xy}) is similar in form. For the sake of brevity, the derivation steps are skipped and the final closed-form expressions are presented in Appendix B.

We now turn our attention to vertical component of scattered electric field due to a y oriented dipole. If we observe equation (22), we can see that there are two S-parameters contributing to $E_{zy}(\vec{r}_o, \vec{r}_d)$. The contribution of S_{21} in polar coordinates is:

$$E_{zy}^{S_{21}}(\vec{r}_o, \vec{r}_d) = \frac{j\omega\mu}{8\pi} \int_0^{+\infty} k_\rho dk_\rho \frac{e^{-jk_z(z_o+z_d)}}{jk_z} \frac{k_\rho}{k_s} S_{21}(k_\rho) \times \frac{1}{\pi} \int_0^{2\pi} d\phi \cos(\phi) e^{-jk_\rho \rho \cos(\phi - \Psi)} \quad (54)$$

After performing the integration with respect to $d\phi$, the following integration which resembles the derivative of Sommerfeld identity is obtained.

$$E_{zy}^{S_{21}}(\vec{r}_o,\vec{r}_d) = \frac{\omega\mu}{4\pi}\cos(\Psi)\int_0^{+\infty}\frac{e^{-jk_z(z_o+z_d)}}{jk_z}\frac{S_{21}(k_\rho)}{k_s} \times J_1(k_\rho\rho)k_\rho^2 dk_\rho \tag{55}$$

Following complex image approximation is made to be able to express the result of the integral in a closed form:

$$\frac{S_{21}(k_\rho)}{k_s} = \sum_{k=1}^{N_4} B_{4k}e^{-jk_z\gamma_{4k}} \tag{56}$$

Utilizing the derivative of Sommerfeld identity yields the following finite sum for $E_{zy}^{S_{21}}(\vec{r}_o,\vec{r}_d)$:

$$E_{zy}^{S_{21}}(\vec{r}_o,\vec{r}_d) = \frac{\omega\mu}{4\pi}\cos(\Psi)\rho\sum_{k=1}^{N_4} B_{4k}(1+jk_sr_{4k})\frac{e^{-jk_sr_{4k}}}{r_{4k}^3} \tag{57}$$

Since $\rho\cos(\Psi) = (x_o - x_d)$, we finally obtain:

$$E_{zy}^{S_{21}}(\vec{r}_o,\vec{r}_d) = \frac{\omega\mu}{4\pi}(x_o - x_d)\sum_{k=1}^{N_4} B_{4k}(1+jk_sr_{4k})\frac{e^{-jk_sr_{4k}}}{r_{4k}^3} \tag{58}$$

where r_{4k} is defined as:

$$r_{4k} = \sqrt{(x_o - x_d)^2 + (y_o - y_d)^2 + (z_o + z_d + \gamma_{4k})^2} \tag{59}$$

A similar derivation applies for the $E_{zy}^{S_{22}}(\vec{r}_o,\vec{r}_d)$ and it is found to be as:

$$E_{zy}^{S_{22}}(\vec{r}_o,\vec{r}_d) = \frac{\omega\mu}{4\pi}(y_o - y_d)\sum_{k=1}^{N_5} B_{5k}(1+jk_sr_{5k})\frac{e^{-jk_sr_{5k}}}{r_{5k}^3} \tag{60}$$

where the following complex image approximation is used:

$$\frac{S_{22}k_z}{k_s^2} = \sum_{k=1}^{N_5} B_{5k}e^{-jk_z\gamma_{5k}} \tag{61}$$

and r_{5k} is defined as:

$$r_{5k} = \sqrt{(x_o - x_d)^2 + (y_o - y_d)^2 + (z_o + z_d + \gamma_{5k})^2} \tag{62}$$

Derivation of the closed-form expressions for a y-directed dipole excitation are presented. Since the reflection coefficients are assumed to be independent of ϕ, the expressions due to an x-directed dipole excitation can be easily obtained with a simple change of variables between x and y. Hence all components of the dyadic Green's function for horizontal sources are available, which makes it possible to analyze planar antennas places over periodic structures.

8 S-parameter related entities ((31), (36), (41), (42), (48), (49), (56), (61)) need to be approximated in terms of a finite summation of complex exponentials, to obtain closed-form expressions for dyadic Green's functions of horizontal sources over periodic structures. These approximations are achieved by sampling the associated entity along a path in complex k_ρ(or k_z) domain. The path used for the sampling in this study is nearly the same as described in [41]. In Fig. 2, C_0 denotes the sampling path defined in [41] and C_1 denotes the path used in this work. The difference is that, one end of the sampling path is not exactly at $k_z = k_s$ as is the case in [41] but instead it is at a slightly shifted point on the real k_z axis. The other end of the path is shifted slightly upwards on the imaginary k_z axis. This modification is made to prevent numerical errors occurring in the approximation process due to the pole at $k_\rho = 0$ for the functions to be approximated. The sampling path is truncated at a point very close to $k_z = -jk_sT$. T is taken as 5 in this work. The justification for this value can be made by observing the exponential inside the inverse Hankel transform integrals above. If dipole and observation point are both at a minimum height of 0.1λ from the periodic structure, then the exponential inside these integrals (e.g., (55)) takes the following value:

$$e^{-jk_z(z_o+z_d)}\Big|_{z_o=z_d=0.1\lambda \text{ and } k_z=-jk_s5} = e^{-k_s\lambda} = e^{-2\pi} \tag{63}$$

which is smaller than 0.002. This ensures that the contribution to the integral from the components with wavenumbers beyond the chosen truncation point is negligible which is also verified by numerical integration accuracy test as will be explained in the next paragraph.

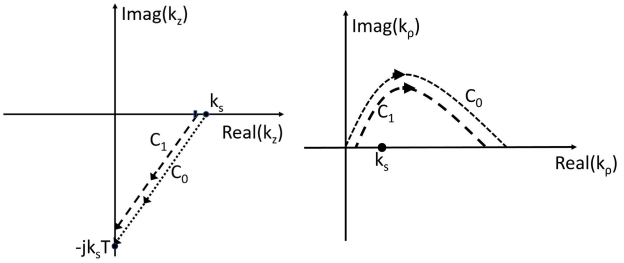

FIGURE 2. Sampling path described in [41] (C_0) and modified sampling path used in the proposed method in this paper (C_1), where T is the sampling truncation number.

At each sample point, the MoM solution of the periodic structure for the corresponding plane wave incidence is performed only once and all required parameters are calculated without any significant additional time cost. Extraction of the complex images from the sampled data is performed by the Generalized Pencil of Function (GPOF) technique [42]. In an intermediate step of this technique, a singular value decomposition (SVD) is applied on the sampled data matrix. Only significant singular values which are larger than a preset threshold value are taken into account, and the number of these significant singular values determines the number of complex exponentials used in the approximation. The threshold value used in this work is

1×10^{-8}, unless stated otherwise. The number of complex images obtained with this criterion varies between 6 and 15 depending on the approximated S-parameter related entity and whether the periodic structure is in free space or in layered media. The accuracy of the DCIM approximation is verified by computing the integrals (e.g., (30), (35)) numerically for a set of source-observation points and comparing these to the integral results calculated through sum of exponentials obtained via DCIM (e.g., (32), (37)). The numeric computation of the integrals are carried out on a path which is C_0 of Fig. 2 extended with a straight path between $k_z = -jk_s5$ and $k_z = -jk_s200$. Highest error in the integral results obtained by DCIM approach is observed to be less than 2.5% which is sufficient for the accuracy of the fields. To demonstrate the accuracy of the formulation proposed in this work, numerical results corresponding to the application of it on some sample problems will be presented in the next section in comparison with the results obtained from a commercially available 3-D electromagnetic simulation software, HFSS by Ansys [43].

III. NUMERICAL RESULTS

Two different cases are considered such that in the first case, the periodic structure is in free space while in the second one the periodic surface is printed on a dielectric slab as an example of a multilayered medium. The sample problem for free space is the same as in Fig. 3 of [32]. However, a comparison of the results with the ones reported in [32] will not be presented since the scattered field results are not available for that work, and the total field values are almost equal to the incident field values of the dipole source without the periodic structure. The periodic structure is a square PEC patch array as shown in Fig. 3 with parameter values presented in Table 1. For multilayered test case, the same patch array is printed on a dielectric slab with dielectric constant of 3.38 and thickness of 2mm. The results for free space (FS) and multilayered (MLYD) cases are presented comparatively on same plots, to observe the effects of the dielectric slab.

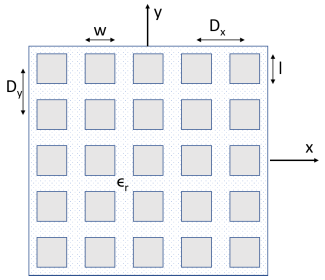

FIGURE 3. Periodic surface.

The selection of this geometry is based on the fact that the S-parameters have negligible dependence on ϕ as observed from the reflection coefficient results for different incident angles presented in Figure 4. Note that this kind of behaviour

TABLE 1. Parameters of the problem.

Parameter	Description	Value
f	frequency	15 GHz
D_x	periodicity in x direction	2 mm (0.1λ)
D_y	periodicity in y direction	2 mm (0.1λ)
w	width of the PEC scatterer	1.8 mm
l	length of the PEC scatterer	1.8 mm

is a requirement to obtain the closed-form Green's function expressions proposed in this work.

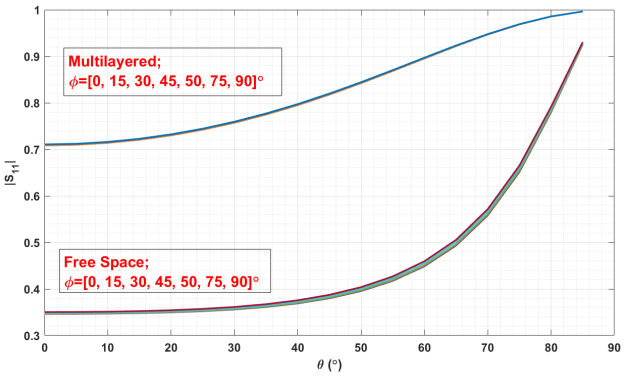

FIGURE 4. Magnitude of S_{11} for the structure described in Fig. 3 and Table 1.

Assuming that the patch array lies at $z = 0$ plane, a y oriented dipole is placed at the center of the periodic structure at a height of 3mm (0.15λ) ($x_d = y_d = 0, z_d = 3mm$). First the variation of E_{yy} with respect to the position of observation point along x (x_o) and y (y_o) directions is examined for different heights (z_o). Figure 5 and 6 respectively show the magnitude and phase of E_{yy} with respect to x_o at $y_o = 0$ and $z_o = 5$ mm (2mm above the dipole). The structure in consideration is infinitely periodic in x and y directions. However for Hertzian dipole excitation, HFSS can provide results only for periodic structures truncated at a finite number of cells. In order to observe the convergence of HFSS results, several simulations are performed for increasing number of cells, and the number of cells used in each direction for the corresponding simulation is denoted by $M \times M$ in the legends of the plots. Since the field variation is slow in x direction, the convergence of HFSS results can not be easily observed from the magnitude plots. However, the phase plots demonstrate that HFSS results converge for 55 number of cells in both x and y directions.

The magnitude and phase variation of E_{yy} with respect to y_o at $x_o = 0$ and $z_o = 5$ are presented in Figures 7 and 8, respectively. As expected from a y directed dipole, the field variation is more rapid in y direction. Again the convergence of HFSS results can be observed better from the phase plots. For both variations with respect to x and y, good agreement between HFSS results and the results obtained with the proposed method are observed for both free space and multilayered cases.

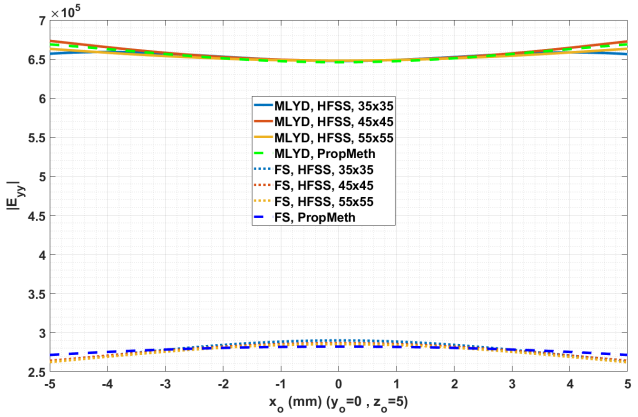

FIGURE 5. Magnitude of E_{yy} with respect to x_o ($y_o = 0$ and $z_o = 5$ mm).

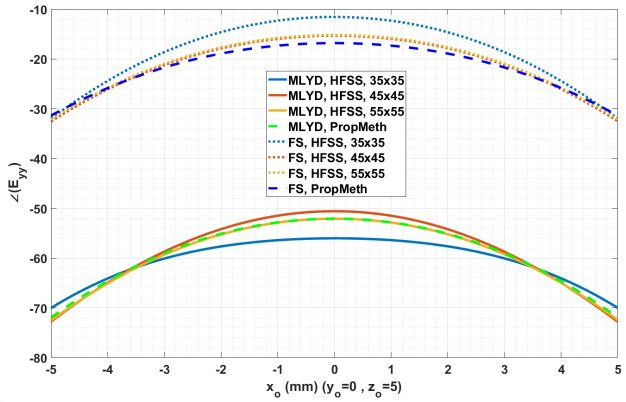

FIGURE 6. Phase of E_{yy} with respect to x_o ($y_o = 0$ and $z_o = 5$ mm).

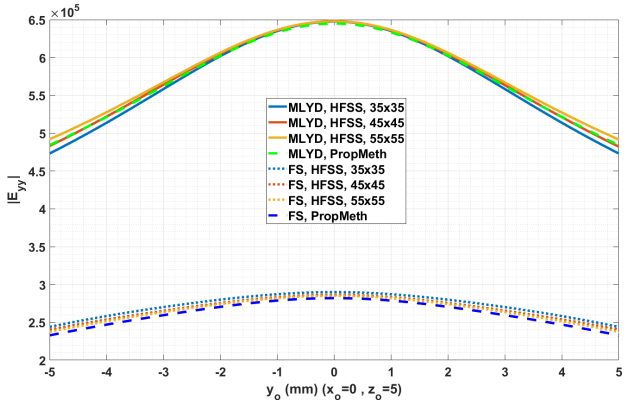

FIGURE 7. Magnitude of E_{yy} with respect to y_o ($x_o = 0$ and $z_o = 5$ mm).

The accuracy of the results become more important as the observation point moves close to the source point. Hence the previous analyses are repeated when the observation point is at $z_o = 2$ mm plane which is 1mm below the dipole source. The magnitude and phase plots for this close proximity case are presented at two orthogonal lines in Figures 9 to 12. Good agreement between the results obtained by the proposed method and HFSS simulation results can still be observed

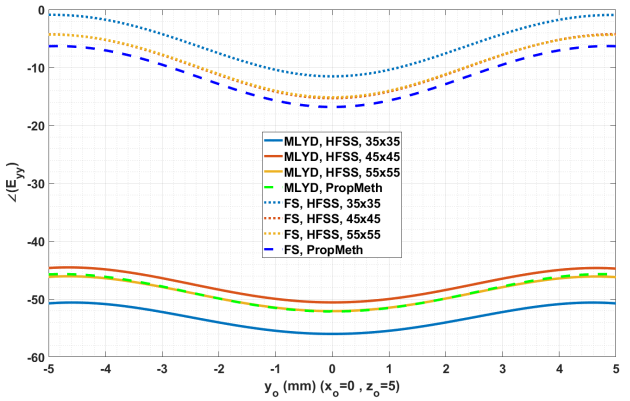

FIGURE 8. Phase of E_{yy} with respect to y_o ($x_o = 0$ and $z_o = 5$ mm).

even though the observation point gets closer to the source and the fields vary much more faster compared to the previous case.

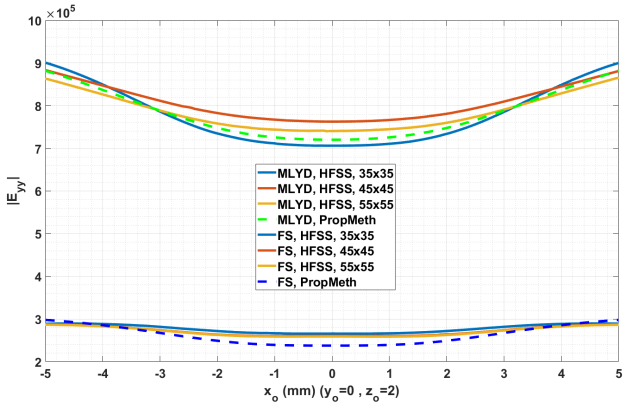

FIGURE 9. Magnitude of E_{yy} with respect to x_o ($y_o = 0$ and $z_o = 2$ mm).

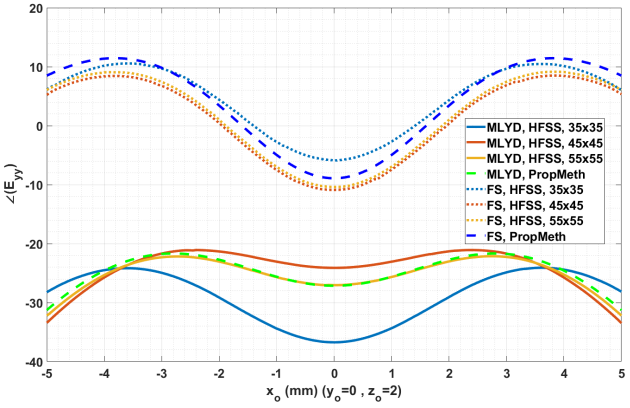

FIGURE 10. Phase of E_{yy} with respect to x_o ($y_o = 0$ and $z_o = 2$ mm).

We now focus on evaluating the results for z component of the scattered electric field due to a y oriented dipole. Recall from the formulation in the previous section that E_{zy} can be seen as a sum of the contributions from S_{21} and S_{22}. Since

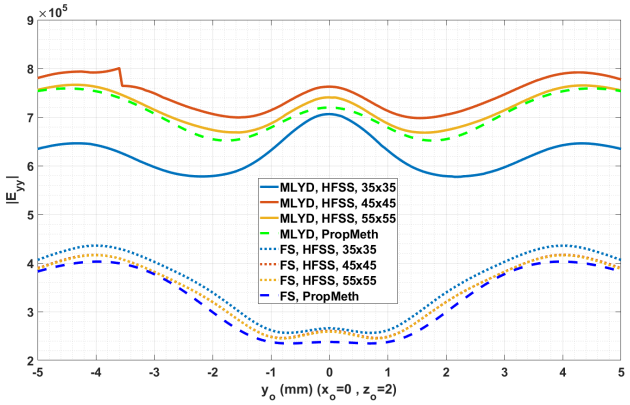

FIGURE 11. Magnitude of E_{yy} with respect to y_o ($x_o = 0$ and $z_o = 2$ mm).

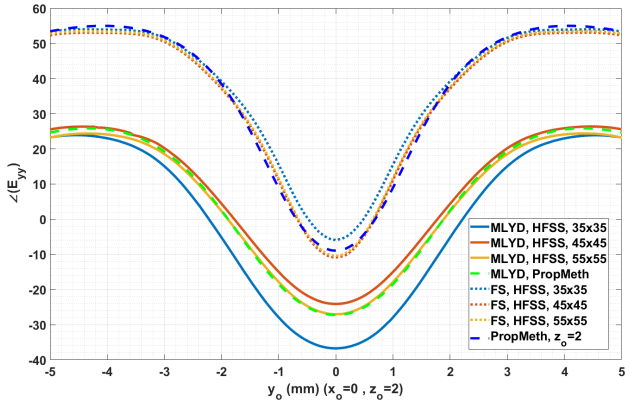

FIGURE 12. Phase of E_{yy} with respect to y_o ($x_o = 0$ and $z_o = 2$ mm).

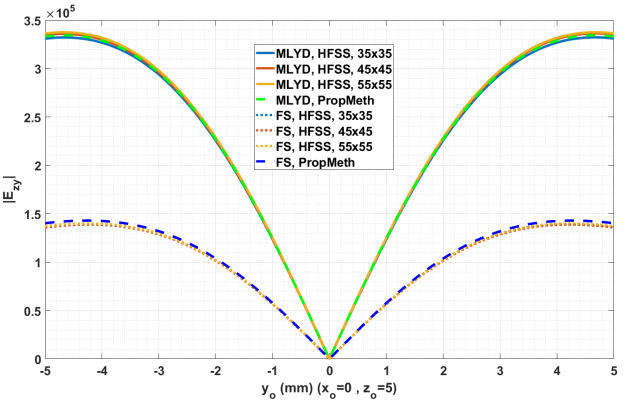

FIGURE 13. Magnitude of E_{zy} with respect to y_o ($x_o = 0$ and $z_o = 5$ mm).

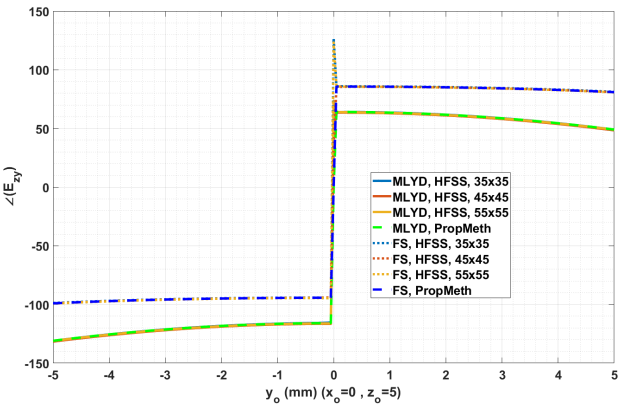

FIGURE 14. Phase of E_{zy} with respect to y_o ($x_o = 0$ and $z_o = 5$ mm).

the cross coupling between TE and TM polarized fields is negligible for the analyzed structure, we end up with only contribution being due to S_{22}. Equation (60) refers that E_{zy} vanishes as y coordinates of the observation point and the dipole source gets closer to each other. Thus, E_{zy} is not plotted along $y_o = 0$ line as it is zero for that case. Magnitude and phase plots for E_{zy} with respect to y_o at two different observation heights ($z = 5$ and $z = 2$) are presented in Figures 13 to 16. It is clearly seen that the results of the proposed approach agrees very well with the results of HFSS for the vertical component of the scattered field as well. Agreement is preserved for both height values of observation plane and for both free space and multilayered cases.

An evaluation of the proposed approach would not be complete without discussing its efficiency. The most time consuming part of the method is the numerical computation of the S-parameters at the sample points for DCIM approximation. The number of samples used for the results presented in this section, is 200 which is seen to be sufficient for converged field values as seen in Fig 17. For free space case, first sampling point requires 2 seconds and each of the other sampling points takes 1.2 seconds resulting a total of 4 minutes time for the calculation of all entries of the dyadic Green's function. For multilayered case, calculations

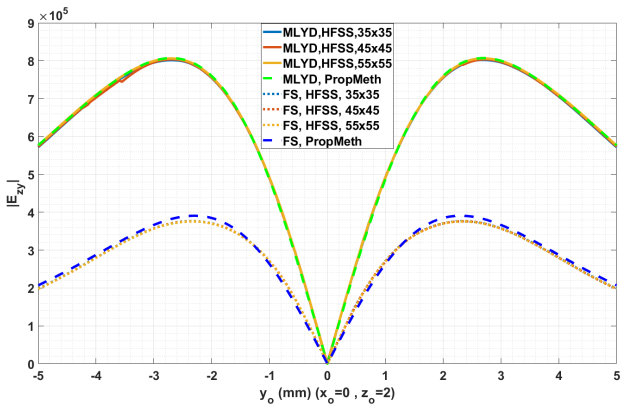

FIGURE 15. Magnitude of E_{zy} with respect to y_o ($x_o = 0$ and $z_o = 2$ mm).

at the initial sampling point takes 40 seconds while the time required for each of the remaining sampling points is 3.5 seconds. This makes a total of 12.3 minute calculation time for all the dyadic Green's function components.

HFSS, on the other hand, requires much more time to yield converged values. For the free space problem with 45×45 unit cells, total time required for HFSS is 8.5 hours while for multilayered problem with the same number of unit cells

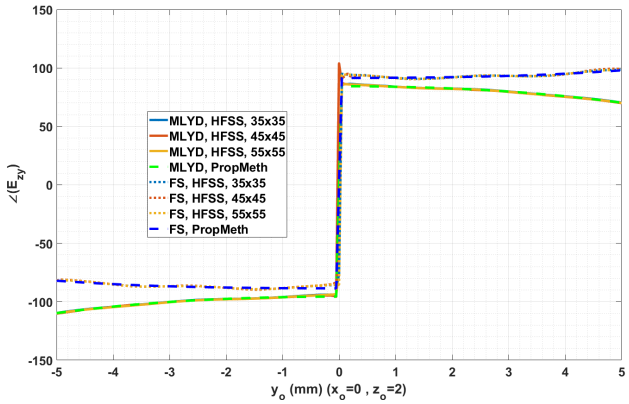

FIGURE 16. Phase of E_{zy} with respect to y_o ($x_o = 0$ and $z_o = 2$ mm).

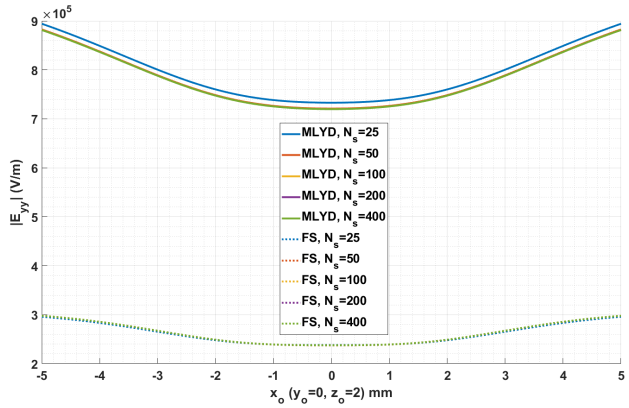

FIGURE 17. Magnitude of E_{yy} with respect to x_o ($y_o = 0$ and $z_o = 2$ mm) for free space (FS) and multilayered (MLYD) problems to demonstrate the convergence of the proposed method with respect to number of samples.

10 hours is required. For the multilayered case, the difference between the results with 45×45 and 55×55 unit cells is more significant compared to the difference for free space problem. If one runs the simulation in HFSS with 55×55 unit cells, then the time required for this goes as high as 27 hours. Proposed method offers an efficiency improvement by a factor of more than 125.

In all of the numerical examples studied in this paper, a work station type of notebook is used with a 128 GB of RAM. The processor of the computer is Intel Core i7-9750H CPU with 2.60GHz clock speed.

IV. CONCLUSION

A novel approach has been presented in this paper to analyze the fields due to electric dipole sources in the vicinity of planar periodic structures. The accuracy of the proposed method is demonstrated with various numerical results including both magnitude and phase of scattered electric fields. The efficiency of the approach is also proven by comparing its computational cost against the simulation time of HFSS for a finite periodic structure large enough to observe convergence of the results.

It is believed that the proposed method will fill an important gap in the literature by obtaining closed-form Green's function expressions for the dipole excitation of periodic planar structures. It eliminates the need for calculating the inverse Fourier transform or Sommerfeld integrals for different source and/or observation point locations. It achieves this efficiency while keeping the accuracy at high levels even for field variations at small scales since it is based on the full-wave MoM solution of reflection coefficients.

APPENDIX A
BESSEL IDENTITIES

Some useful identities and transform equations utilized in the formulation of the approach proposed in this paper are summarized from [44] and [45]. The Sommerfeld identity is given as:

$$\frac{e^{-jk_s r}}{r} = \int_0^\infty \frac{e^{-jk_z z}}{jk_z} J_0(k_\rho \rho) k_\rho dk_\rho \tag{64}$$

where $J_0(z)$ is the Bessel function of the first kind of order 0. The derivative of the Sommerfeld identity with respect to ρ is

$$\rho(1 + jk_s r)\frac{e^{-jk_s r}}{r^3} = \int_0^\infty \frac{e^{-jk_z z}}{jk_z} J_1(k_\rho \rho) k_\rho^2 dk_\rho \tag{65}$$

In order to reach (65) from (64), the following identity of Bessel function is used.

$$\frac{d}{dz}[z^{-\nu} J_\nu(z)] = -z^{-\nu} J_{\nu+1}(z) \tag{66}$$

A useful integral representation of Bessel function of the first kind of integer order n is given as:

$$J_n(z) = \frac{j^{-n}}{2\pi} \int_0^{2\pi} e^{jz\cos\phi} e^{jn\phi} d\phi \tag{67}$$

The recurrence relations are used to relate Bessel functions of different orders. A very useful one of them is given as follows:

$$J_{\nu-1}(z) + J_{\nu+1}(z) = \frac{2\nu}{z} J_\nu(z) \tag{68}$$

Identities for negative argument and negative integer order are also worth mentioning as these are among the mostly used Bessel identities.

$$\begin{aligned} J_{-n}(z) &= (-1)^n J_n(z) \\ J_n(-z) &= (-1)^n J_n(z) \end{aligned} \tag{69}$$

APPENDIX B
CLOSED-FORM EXPRESSION FOR E_{xy}

By observing the similarities and differences in the expressions for contributions of S-parameters to the electric field components in equations (19) through (21), one can quickly

determine the closed-form expressions for E_{xy}, which are given below:

$$E_{xy}^{S_{11}}(\vec{r}_o,\vec{r}_d) = E_{xy}^{S_{11}:I_a}(\vec{r}_o,\vec{r}_d) + E_{xy}^{S_{11}:I_b}(\vec{r}_o,\vec{r}_d) \tag{70}$$

$$E_{xy}^{S_{11}:I_a}(\vec{r}_o,\vec{r}_d) = \frac{j\omega\mu}{8\pi}\sin(2\Psi)\sum_{k=1}^{N_1} B_{1k}\frac{e^{-jk_s r_{1k}}}{r_{1k}} \tag{71}$$

$$E_{xy}^{S_{11}:I_b}(\vec{r}_o,\vec{r}_d) = -\frac{j\omega\mu}{4\pi}\sin(2\Psi)\sum_{k=1}^{N_{a1}} B_{a1k}(1+jk_s r_{a1k}) \times \frac{e^{-jk_s r_{a1k}}}{r_{a1k}^3} \tag{72}$$

$$E_{xy}^{S_{21}}(\vec{r}_o,\vec{r}_d) = E_{xy}^{S_{21}:I_1}(\vec{r}_o,\vec{r}_d) + E_{xy}^{S_{21}:I_{2a}}(\vec{r}_o,\vec{r}_d) + E_{xy}^{S_{21}:I_{2b}}(\vec{r}_o,\vec{r}_d) \tag{73}$$

$$E_{xy}^{S_{21}:I_1}(\vec{r}_o,\vec{r}_d) = -\frac{j\omega\mu}{8\pi}\sum_{k=1}^{N_2} B_{2k}\frac{e^{-jk_s r_{2k}}}{r_{2k}} \tag{74}$$

$$E_{xy}^{S_{21}:I_{2a}}(\vec{r}_o,\vec{r}_d) = -\frac{j\omega\mu}{8\pi}\cos(2\Psi)\sum_{k=1}^{N_2} B_{2k}\frac{e^{-jk_s r_{2k}}}{r_{2k}} \tag{75}$$

$$E_{xy}^{S_{21}:I_{2b}}(\vec{r}_o,\vec{r}_d) = \frac{j\omega\mu}{4\pi}\cos(2\Psi)\sum_{k=1}^{N_{a2}} B_{a2k}(1+jk_s r_{a2k}) \times \frac{e^{-jk_s r_{a2k}}}{r_{a2k}^3} \tag{76}$$

$$E_{xy}^{S_{12}}(\vec{r}_o,\vec{r}_d) = E_{xy}^{S_{12}:I_1}(\vec{r}_o,\vec{r}_d) + E_{xy}^{S_{12}:I_{2a}}(\vec{r}_o,\vec{r}_d) + E_{xy}^{S_{12}:I_{2b}}(\vec{r}_o,\vec{r}_d) \tag{77}$$

$$\begin{aligned} E_{xy}^{S_{12}:I_1}(\vec{r}_o,\vec{r}_d) &= -E_{xy}^{S_{21}:I_1}(\vec{r}_o,\vec{r}_d) \\ E_{xy}^{S_{12}:I_{2a}}(\vec{r}_o,\vec{r}_d) &= E_{xy}^{S_{21}:I_{2a}}(\vec{r}_o,\vec{r}_d) \\ E_{xy}^{S_{12}:I_{2b}}(\vec{r}_o,\vec{r}_d) &= E_{xy}^{S_{21}:I_{2b}}(\vec{r}_o,\vec{r}_d) \end{aligned} \tag{78}$$

$$E_{xy}^{S_{22}}(\vec{r}_o,\vec{r}_d) = E_{xy}^{S_{22}:I_a}(\vec{r}_o,\vec{r}_d) + E_{xy}^{S_{22}:I_b}(\vec{r}_o,\vec{r}_d) \tag{79}$$

$$E_{xy}^{S_{22}:I_a}(\vec{r}_o,\vec{r}_d) = -\frac{j\omega\mu}{8\pi}\sin(2\Psi)\sum_{k=1}^{N_3} B_{3k}\frac{e^{-jk_s r_{3k}}}{r_{3k}} \tag{80}$$

$$E_{xy}^{S_{22}:I_b}(\vec{r}_o,\vec{r}_d) = \frac{j\omega\mu}{4\pi}\sin(2\Psi)\sum_{k=1}^{N_{a3}} B_{a3k}(1+jk_s r_{a3k}) \times \frac{e^{-jk_s r_{a3k}}}{r_{a3k}^3} \tag{81}$$

REFERENCES

[1] D. Sievenpiper, L. Zhang, R. F. J. Broas, N. G. Alexopolous, and E. Yablonovitch, "High-impedance electromagnetic surfaces with a forbidden frequency band," *IEEE Trans. Microw. Theory Techn.*, vol. 47, no. 11, pp. 2059–2074, Nov. 1999, doi: 10.1109/22.798001.

[2] F. Yang and Y. Rahmat-Samii, "Reflection phase characterizations of the EBG ground plane for low profile wire antenna applications," *IEEE Trans. Antennas Propag.*, vol. 51, no. 10, pp. 2691–2703, Oct. 2003, doi: 10.1109/TAP.2003.817559.

[3] A. P. Feresidis, G. Goussetis, S. Wang, and J. C. Vardaxoglou, "Artificial magnetic conductor surfaces and their application to low-profile high-gain planar antennas," *IEEE Trans. Antennas Propag.*, vol. 53, no. 1, pp. 209–215, Jan. 2005, doi: 10.1109/TAP.2004.840528.

[4] Y. Zhang, J. von Hagen, M. Younis, C. Fischer, and W. Wiesbeck, "Planar artificial magnetic conductors and patch antennas," *IEEE Trans. Antennas Propag.*, vol. 51, no. 10, pp. 2704–2712, Oct. 2003, doi: 10.1109/TAP.2003.817550.

[5] H. Mosallaei and K. Sarabandi, "Antenna miniaturization and bandwidth enhancement using a reactive impedance substrate," *IEEE Trans. Antennas Propag.*, vol. 52, no. 9, pp. 2403–2414, Sep. 2004, doi: 10.1109/TAP.2004.834135.

[6] R. F. J. Broas, D. F. Sievenpiper, and E. Yablonovitch, "An application of high-impedance ground planes to phased array antennas," *IEEE Trans. Antennas Propag.*, vol. 53, no. 4, pp. 1377–1381, Apr. 2005, doi: 10.1109/TAP.2005.844408.

[7] M. Li, S.-Q. Xiao, and B.-Z. Wang, "Investigation of using high impedance surfaces for wide-angle scanning arrays," *IEEE Trans. Antennas Propag.*, vol. 63, no. 7, pp. 2895–2901, Jul. 2015, doi: 10.1109/TAP.2015.2421936.

[8] M. Li, S.-Q. Xiao, J. Xiong, and B.-Z. Wang, "Horizontal dipole located close to ground plane with bidirectional endfire radiation," *IEEE Antennas Wireless Propag. Lett.*, vol. 13, pp. 1144–1147, 2014, doi: 10.1109/LAWP.2014.2331104.

[9] M. Li, S.-Q. Xiao, Z. Wang, and B.-Z. Wang, "Compact surface-wave assisted beam-steerable antenna based on HIS," *IEEE Trans. Antennas Propag.*, vol. 62, no. 7, pp. 3511–3519, Jul. 2014, doi: 10.1109/TAP.2014.2321161.

[10] Z. L. Ma and C. H. Chan, "A novel surface-wave-based high-impedance surface multibeam antenna with full azimuth coverage," *IEEE Trans. Antennas Propag.*, vol. 65, no. 4, pp. 1579–1588, Apr. 2017, doi: 10.1109/TAP.2017.2670320.

[11] J. Tamura, H. Arai, and T. Itoh, "High-impedance surface-based null-steering antenna for angle-of-arrival estimation," *IEEE Trans. Antennas Propag.*, vol. 70, no. 5, pp. 3269–3276, May 2022, doi: 10.1109/TAP.2021.3137469.

[12] F. Capolino, D. R. Jackson, D. R. Wilton, and L. B. Felsen, "Comparison of methods for calculating the field excited by a dipole near a 2-D periodic material," *IEEE Trans. Antennas Propag.*, vol. 55, no. 6, pp. 1644–1655, Jun. 2007, doi: 10.1109/TAP.2007.897348.

[13] N. Kinayman and M. I. Aksun, *Modern Microwave Circuits*. Boston, MA, USA: Artech House, 2005.

[14] R. Sigelmann and A. Ishimaru, "Radiation from periodic structures excited by an aperiodic source," *IEEE Trans. Antennas Propag.*, vol. AP-13, no. 3, pp. 354–364, May 1965, doi: 10.1109/TAP.1965.1138437.

[15] V. Galindo and C. Wu, "Asymptotic behavior of the coupling coefficients for an infinite array of thin-walled rectangular waveguides," *IEEE Trans. Antennas Propag.*, vol. AP-14, no. 2, pp. 248–249, Mar. 1966, doi: 10.1109/TAP.1966.1138647.

[16] B. Munk and G. Burrell, "Plane-wave expansion for arrays of arbitrarily oriented piecewise linear elements and its application in determining the impedance of a single linear antenna in a lossy half-space," *IEEE Trans. Antennas Propag.*, vol. AP-27, no. 3, pp. 331–343, May 1979, doi: 10.1109/TAP.1979.1142089.

[17] F. Capolino, D. R. Jackson, and D. R. Wilton, "Fundamental properties of the field at the interface between air and a periodic artificial material excited by a line source," *IEEE Trans. Antennas Propag.*, vol. 53, no. 1, pp. 91–99, Jan. 2005, doi: 10.1109/TAP.2004.840518.

[18] S. Paulotto, G. Lovat, P. Baccarelli, and P. Burghignoli, "Green's function calculation for a line source exciting a 2-D periodic printed structure," *IEEE Microw. Wireless Compon. Lett.*, vol. 20, no. 4, pp. 181–183, Apr. 2010, doi: 10.1109/LMWC.2010.2042542.

[19] T. B. Senior and J. Volakis, *Approximate Boundary Conditions in Electromagnetics*. London, U.K.: Institute of Electrical Engineers, 1995.

[20] E. F. Kuester, M. A. Mohamed, M. Piket-May, and C. L. Holloway, "Averaged transition conditions for electromagnetic fields at a metafilm," *IEEE Trans. Antennas Propag.*, vol. 51, no. 10, pp. 2641–2651, Oct. 2003, doi: 10.1109/TAP.2003.817560.

[21] C. L. Holloway, M. A. Mohamed, E. F. Kuester, and A. Dienstfrey, "Reflection and transmission properties of a metafilm: With an application to a controllable surface composed of resonant particles," *IEEE Trans. Electromagn. Compat.*, vol. 47, no. 4, pp. 853–865, Nov. 2005, doi: 10.1109/TEMC.2005.853719.

[22] C. L. Holloway, A. Dienstfrey, E. F. Kuester, J. F. O'Hara, A. K. Azad, and A. J. Taylor, "A discussion on the interpretation and characterization of metafilms/metasurfaces: The two-dimensional equivalent of metamaterials," *Metamaterials*, vol. 3, no. 2, pp. 100–112, Oct. 2009, doi: 10.1016/j.metmat.2009.08.001.

[23] C. L. Holloway and E. F. Kuester, "A homogenization technique for obtaining generalized sheet-transition conditions for a metafilm embedded in a magnetodielectric interface," *IEEE Trans. Antennas Propag.*, vol. 64, no. 11, pp. 4671–4686, Nov. 2016, doi: 10.1109/TAP.2016.2600764.
[24] C. L. Holloway and E. F. Kuester, "Generalized sheet transition conditions for a metascreen—A fishnet metasurface," *IEEE Trans. Antennas Propag.*, vol. 66, no. 5, pp. 2414–2427, May 2018, doi: 10.1109/TAP.2018.2809620.
[25] C. L. Holloway, E. F. Kuester, and A. H. Haddab, "Retrieval approach for determining surface susceptibilities and surface porosities of a symmetric metascreen from reflection and transmission coefficients," *Prog. Electromagn. Res.*, vol. 166, pp. 1–22, 2019, doi: 10.2528/pier19022305.
[26] C. L. Holloway, E. F. Kuester, and A. H. Haddab, "Using reflection and transmission coefficients to retrieve surface parameters for an anisotropic metascreen: With a discussion on conversion between TE and TM polarizations," *J. Appl. Phys.*, vol. 125, no. 9, 2019, Art. no. 095102, doi: 10.1063/1.5050987.
[27] S. Tretyakov, *Analytical Modeling in Applied Electromagnetics*. Boston, MA, USA: Artech House, 2003.
[28] S. A. Tretyakov, A. J. Viitanen, S. I. Maslovski, and I. E. Saarela, "Impedance boundary conditions for regular dense arrays of dipole scatterers," *IEEE Trans. Antennas Propag.*, vol. 51, no. 8, pp. 2073–2078, Aug. 2003, doi: 10.1109/TAP.2003.814737.
[29] O. Luukkonen, C. Simovski, G. Granet, G. Goussetis, D. Lioubtchenko, A. V. Raisanen, and S. A. Tretyakov, "Simple and accurate analytical model of planar grids and high-impedance surfaces comprising metal strips or patches," *IEEE Trans. Antennas Propag.*, vol. 56, no. 6, pp. 1624–1632, Jun. 2008, doi: 10.1109/TAP.2008.923327.
[30] G. Lovat, "Near-field shielding effectiveness of 1-D periodic planar screens with 2-D near-field sources," *IEEE Trans. Electromagn. Compat.*, vol. 51, no. 3, pp. 708–719, Aug. 2009, doi: 10.1109/TEMC.2009.2022273.
[31] S. Paulotto, P. Baccarelli, P. Burghignoli, G. Lovat, G. W. Hanson, and A. B. Yakovlev, "Homogenized Green's functions for an aperiodic line source over planar densely periodic artificial impedance surfaces," *IEEE Trans. Microw. Theory Techn.*, vol. 58, no. 7, pp. 1807–1817, Jul. 2010, doi: 10.1109/TMTT.2010.2049917.
[32] F. Liang, G. W. Hanson, A. B. Yakovlev, G. Lovat, P. Burghignoli, R. Araneo, and S. A. Hassani Gangaraj, "Dyadic Green's functions for dipole excitation of homogenized metasurfaces," *IEEE Trans. Antennas Propag.*, vol. 64, no. 1, pp. 167–178, Jan. 2016, doi: 10.1109/TAP.2015.2501430.
[33] A. Azari, Z. H. Firouzeh, and A. Bakhtafrouz, "Homogenized dyadic potential Green's function for planar metasurface placed at two half spaces interface excited by vertical and horizontal ideal electric dipole," *IEEE Trans. Antennas Propag.*, vol. 68, no. 4, pp. 2965–2974, Apr. 2020, doi: 10.1109/TAP.2019.2963212.
[34] A. Azari, Z. H. Firouzeh, and A. Bakhtafrouz, "Field calculation of electric dipole excitation of a metafilm printed on a finite-thickness dielectric slab using the susceptibility homogenization method," *IET Microw., Antennas Propag.*, vol. 15, no. 5, pp. 503–510, 2021, doi: 10.1049/mia2.12076.
[35] A. K. Bhattacharyya, *Phased Array Antennas: Floquet Analysis, Synthesis, BFNs and Active Array Systems*. Hoboken, NJ, USA: Wiley, 2006.
[36] C.-C. Chen, "Scattering by a two-dimensional periodic array of conducting plates," *IEEE Trans. Antennas Propag.*, vol. AP-18, no. 5, pp. 660–665, Sep. 1970, doi: 10.1109/TAP.1970.1139760.
[37] S. Rao, D. Wilton, and A. Glisson, "Electromagnetic scattering by surfaces of arbitrary shape," *IEEE Trans. Antennas Propag.*, vol. AP-30, no. 3, pp. 409–418, May 1982, doi: 10.1109/TAP.1982.1142818.
[38] A. Alparslan, M. I. Aksun, and K. A. Michalski, "Closed-form Green's functions in planar layered media for all ranges and materials," *IEEE Trans. Microw. Theory Techn.*, vol. 58, no. 3, pp. 602–613, Mar. 2010.
[39] K. E. Jordan, G. R. Richter, and P. Sheng, "An efficient numerical evaluation of the Green's function for the Helmholtz operator on periodic structures," *J. Comput. Phys.*, vol. 63, no. 1, pp. 222–235, Mar. 1986.
[40] S. Adanir and L. Alatan, "Complete and accurate discrete complex image approximation of periodic Green's function in layered media," *IEEE Trans. Antennas Propag.*, vol. 62, no. 8, pp. 4115–4121, Aug. 2014, doi: 10.1109/TAP.2014.2323087.
[41] Y. L. Chow, J. J. Yang, D. G. Fang, and G. E. Howard, "A closed-form spatial Green's function for the thick microstrip substrate," *IEEE Trans. Microw. Theory Techn.*, vol. 39, no. 3, pp. 588–592, Mar. 1991, doi: 10.1109/22.75309.
[42] Y. Hua and T. K. Sarkar, "Generalized pencil-of-function method for extracting poles of an EM system from its transient response," *IEEE Trans. Antennas Propag.*, vol. 37, no. 2, pp. 229–234, Feb. 1989, doi: 10.1109/8.18710.
[43] *HFSS*. Accessed: Jul. 6, 2023. [Online]. Available: https://www.ansys.com/products/electronics/ansys-hfss
[44] A. D. Poularikas, Ed., *Transforms and Applications Handbook*. 3rd ed. Boca Raton, FL, USA: CRC Press, 2010.
[45] F. W. J. Olver, D. W. Lozier, R. F. Boisvert, and C. W. Clark, Eds., *NIST Handbook of Mathematical Functions*. Cambridge, U.K.: Cambridge Univ. Press, 2010.

SÜLEYMAN ADANIR received the B.Sc., M.Sc., and Ph.D. degrees in electrical and electronics engineering (EEE) from Middle East Technical University (METU), Ankara, Turkey, in 2008, 2011, and 2022, respectively. He was a RF/MW Design Engineer with Aselsan, Turkey, from 2008 to 2022. Since 2022, he has been a RF Systems Engineer with Forefront RF, Cambridge, U.K. His research interests include computational electromagnetics, analysis of periodic structures, software-defined radios, and mobile communications.

LALE ALATAN (Member, IEEE) received the B.Sc., M.Sc., and Ph.D. degrees in electrical and electronics engineering (EEE) from Middle East Technical University (METU), Ankara, Turkey, in 1990, 1993, and 1997, respectively. She was a Postdoctoral Visiting Research Associate with the Electrical and Computer Engineering (ECE) Department, Carnegie Mellon University, and New Jersey Institute of Technology (NJIT), from 1997 to 2000. Since 2000, she has been a Faculty Member with the EEE Department, METU. Her research interests include the analysis and design of antenna and antenna arrays, reconfigurable antennas, computational electromagnetics, analysis of periodic structures, and microwave imaging.